International Journal of GEOMATE, July, 2024 Vol.27, Issue 119, pp.1-9
ISSN: 2186-2982 (P), 2186-2990 (O), Japan, DOI: https://doi.org/10.21660/2024.119.g13316
Geotechnique, Construction Materials and Environment

INCORPORATING POISSON EFFECT INTO DEM FOR ENHANCED NUMERICAL ANALYSIS OF MASONRY STRUCTURES

*Aiko Furukawa[1] and Masato Goto[1]

[1] Department of Urban Management, Kyoto University, Japan

*Corresponding Author, Received: 13 June 2023, Revised: 25 April 2024, Accepted: 27 April 2024

ABSTRACT: In the distinct element method (DEM), a structure is modeled as an assembly of rigid elements, and the failure of the structure is represented by the breakage of the springs that connect the elements. The original DEM has a drawback in that spring constants cannot be theoretically determined. The refined DEM solved this problem and made the spring constant possible to be theoretically determined from material properties. However, the refined DEM still has a drawback in that the Poisson effect cannot be considered, and it cannot represent the tensile stress/strain and tensile failure in the orthogonal direction of the compressive force. This study proposes a method to introduce the Poisson effect into the refined DEM that can consider tensile stress/strain or tensile failure due to the Poisson effect. Since the non-diagonal component of the elasticity tensor expresses the Poisson effect, the Poisson effect is introduced using the element stiffness matrix developed using the non-diagonal component of the elasticity tensor. Through numerical analysis of the compression test of a concrete block, it was confirmed that the Poisson's ratio value was quantitatively reproduced, and tensile cracks were qualitatively reproduced.

Keywords: Refined DEM, Poisson effect, Tensile failure, FEM, Element stiffness matrix, Elasticity tensor

1. INTRODUCTION

Masonry structures are widely built, especially in developing countries, due to their low construction cost. However, many masonry structures have collapsed during past earthquakes due to their low seismic resistance, resulting in the loss of many lives [1]. It is important to understand the damage occurrence mechanism of masonry structures during earthquakes and to develop effective reinforcing measures to reduce structural collapse and associated casualties. Various studies have been conducted to achieve this goal, i.e., post-earthquake field survey and damage evaluation [2], pre-earthquake survey to prepare for future earthquakes [3], experimental investigation [4], and numerical analysis [5][6]. The numerical analysis is crucial in understanding the damage occurrence mechanism and developing effective countermeasures. However, a numerical analysis method suitable for masonry structures has not been established.

Numerical analysis methods for structural failure behavior can be divided into two categories: those based on a continuum and those based on dis-continuum.

The FEM (finite element method) [7] is a typical analysis method based on a continuum. The original FEM uses a continuous shape function, making it difficult to represent the failure behavior. Then the FEM using discontinuous shape functions has been developed to represent failure behavior [8]. Attempts have been made to reproduce failure behavior by treating masonry bricks/blocks as discrete bodies using a contact analysis function of the FEM [9]. However, it is still difficult to stably calculate the three-dimensional failure behavior of masonry structures. Apart from the FEM, the mesh-free method [10][11][12] is also a continuum-based method that is good at simulating arbitrary evolving cracks [13]. However, the application to the three-dimensional collapse behavior is still limited.

The DEM (distinct element method) [14] is a typical analysis method based on dis-continuum. In the DEM, the structure is modeled as an assembly of rigid elements, and the elements are connected by springs. The elements themselves do not deform, but the overlapping of the elements represents the deformation of the entire structure, and failure can be easily represented by the disconnection of the springs. The conventional DEM has the problem that the spring constants between elements cannot be theoretically determined, except for spherical and circular elements. The refined DEM [15] discretizes the contact surfaces so that the spring constants can be theoretically determined from the material properties. The refined DEM can reproduce the three-dimensional behavior of masonry structures, i.e., elastic, failure, and collapse behaviors during an earthquake. However, the refined DEM has the problem of being unable to represent the Poisson effect.

Lourenco et al. [16] classified the failure patterns of masonry bricks into several categories, as shown in Fig. 1. The arrows in Fig. 1 represent the direction of force acting on the masonry bricks.

Figures 1(a) and (b) show tensile and shear failures at a joint due to tensile and shear forces, which can be represented by cutting the normal and tangential springs between two elements. Figure 1(c) shows tensile cracks due to the Poisson effect under the compressive force, which the refined DEM cannot reproduce. The refined DEM using rigid elements can reproduce the shrinkage due to compression by the overlap of rigid elements, but it cannot represent the Poisson effect. Past studies that modeled the distinct elements as deformable bodies instead of rigid bodies can automatically express the Poisson effect [17][18]. However, the methods are less stable, like the FEM dealing with the discrete bodies using a contact analysis function.

This study proposes a method to introduce the Poisson effect into the refined DEM. The element stiffness matrix of the FEM due to the Poisson effect was developed from the non-diagonal component of the elasticity tensor, and the force caused by the Poisson effect was added to the discrete elements. Since the failure pattern shown in Fig. 1(c) is an important failure pattern of masonry structures, it is important to develop an analysis method that can simulate this failure pattern.

The proposed method was verified by confirming whether it could reproduce the Poisson effect and the tensile failure caused by the compressive force, as shown in Fig. 1(c). The refined DEM code written by the first author was used in this paper.

2. RESEARCH SIGNIFICANCE

The refined DEM can simulate structural failure behavior and is suitable for the numerical analysis of masonry structures. However, it cannot express the Poisson effect, so one of the typical failure patterns of masonry structures cannot be simulated.

The significance of this study is proposing a method to introduce the Poisson effect into the refined DEM. The Poisson effect is important to simulate the failure pattern shown in Fig. 1(c). The Poisson effect is introduced using the element stiffness matrix of the FEM. The non-diagonal component of the elasticity tensor expresses the Poisson effect. This study develops the element stiffness matrix owing to the Poisson effect using the non-diagonal component of the elasticity tensor, and the force caused by the Poisson effect is computed and applied to the distinct elements.

3. REFINED DISTINCT ELEMENT METHOD

3.1 Overview

In the refined DEM [15], a structure is modeled as an assembly of rigid elements. Interaction between elements is modeled with springs and dashpots attached to the surfaces of elements.

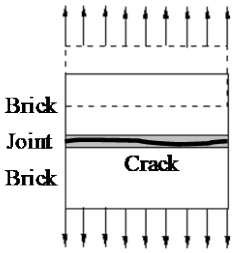

(a) Joint tension cracking due to tensile force

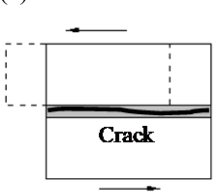

(b) Joint slip due to shear force

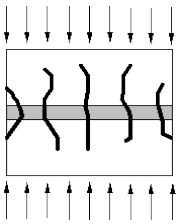

(c) Splitting of bricks in tension as a result of compressive force

Fig.1 Failure patterns of masonry bricks [15]

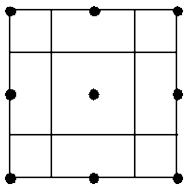

(a) Segments and their representative points on element surface

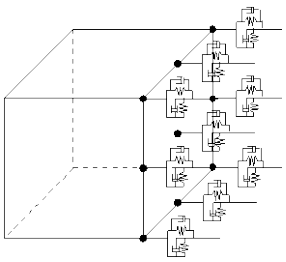

(b) Spring and dashpot attached to representative point of each segment

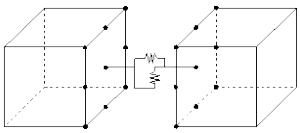

(c)Restoring spring

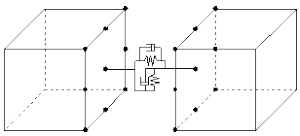

(d) Contact spring and contact dashpot

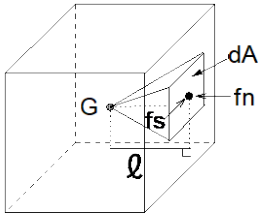

(e) Pyramid composed of elemental gravity center and each segment for deriving the spring constant

Fig.2 Modeling of a spring and dashpot between elements in the refined DEM

The surface of an element is divided into small segments, as shown in Fig. 2 (a). The black points indicate the representative point of each segment. One restoring spring and one combination of contact spring and dashpot are attached to one segment (Fig. 2 (b)) at each of the representative points in Fig. 2 (a). The spring constant for each segment is derived based on the three-dimensional stress-strain relationship of the material and the segment area.

Figure 2 (c) shows a spring for computing the restoring force (restoring spring), which models the elasticity of elements. The restoring spring is set between continuous elements. Structural failure is modeled as the breakage of the restoring spring, at which time the restoring spring is replaced with a contact spring and a contact dashpot. Figure 2 (d) shows a spring and dashpot for computing the contact force (contact spring and dashpot), which models the contact, separation, and re-contact between elements. The dashpots are introduced to express energy dissipation due to the contact.

3.2 Spring Constant of Each Spring

There are two types of springs, namely the restoring and contact springs. The same values are used for these springs. The springs are set for both the normal direction (k_n) and shear (tangential) direction (k_s) of the surface. The subscripts n and s indicate the values in the normal and shear directions. The spring constant of each spring is derived, assuming the equilibrium of force for each pyramid composed of a segment and the gravity center of the element (Fig. 2 (e)). Here, the derivation of the spring constant of each pyramid is described.

Let $\sigma_n(n)$ and $\tau_{ns}(n)$ be the average normal and shear stresses in the pyramid at a distance n from the surface. The variable n is the distance in the direction normal to the surface, and $s(0) = dA$. Let ℓ be the distance from the surface to the gravity center. The average stress can be expressed as

$$\sigma_n(n) = f_n / s(n) \qquad \tau_{ns}(n) = f_s / s(n). \tag{1}$$

The forces f_n and f_s are written as

$$f_n = \sigma_n(n)s(n) \qquad f_s = \tau_{ns}(n)s(n). \tag{2}$$

Since the forces f_n and f_s are constant in the normal direction, Eq. (2) can be rewritten as

$$\begin{aligned} f_n &= \frac{1}{\ell}\int_0^{\ell}\sigma_n(n)s(n)dn = \frac{1}{\ell}\int_V \sigma_n(n)dV \\ f_s &= \frac{1}{\ell}\int_0^{\ell}\tau_{ns}(n)s(n)dn = \frac{1}{\ell}\int_V \tau_{ns}(n)dV \end{aligned} \tag{3}$$

where $\int_V$ indicates volume integration.

The new orthogonal coordinates are defined as (n, s, p). n is the direction perpendicular to the surface as already defined, s is the tangential direction in which the shear force f_s acts, and p is the other tangential direction of the surface in which no force acts. The strain–stress relationship in three dimensions can be written using these coordinates as follows.

$$\begin{Bmatrix} \varepsilon_n \\ \varepsilon_s \\ \varepsilon_p \\ \gamma_{ns} \\ \gamma_{sp} \\ \gamma_{pn} \end{Bmatrix} = \frac{1}{E}\begin{bmatrix} 1 & -\nu & -\nu & 0 & 0 & 0 \\ -\nu & 1 & -\nu & 0 & 0 & 0 \\ -\nu & -\nu & 1 & 0 & 0 & 0 \\ 0 & 0 & 0 & 2(1+\nu) & 0 & 0 \\ 0 & 0 & 0 & 0 & 2(1+\nu) & 0 \\ 0 & 0 & 0 & 0 & 0 & 2(1+\nu) \end{bmatrix}\begin{Bmatrix} \sigma_n \\ \sigma_s \\ \sigma_p \\ \tau_{ns} \\ \tau_{sp} \\ \tau_{pn} \end{Bmatrix} \tag{4}$$

where σ and τ are the normal and shear stresses and ε and γ are the normal and shear strains. E is Young's modulus, and ν is Poisson's ratio of the element (e.g., brick).

Since no force is acting in the p direction, the stresses in the p direction are set to zero.

$$\sigma_p = 0 \quad \tau_{sp} = \tau_{pn} = 0 \tag{5}$$

Therefore, substituting Eq. (5) into Eq. (4) yields

$$\begin{aligned} &\varepsilon_n = \frac{1}{E}(\sigma_n - \nu\sigma_s) \quad \varepsilon_s = \frac{1}{E}(\sigma_s - \nu\sigma_n) \\ &\gamma_{ns} = \frac{2(1+\nu)}{E}\tau_{ns} \\ &\varepsilon_p = \frac{-\nu}{E}(\sigma_n + \sigma_s) \quad \gamma_{sp} = 0 \quad \gamma_{pn} = 0 \end{aligned} \tag{6}$$

The following stress-strain equations are obtained by solving Eq. (6) for σ_n, σ_s, and τ_{ns}.

$$\begin{aligned} \sigma_n &= \frac{E}{1-\nu^2}\varepsilon_n + \frac{E\nu}{1-\nu^2}\varepsilon_s \\ \sigma_s &= \frac{E\nu}{1-\nu^2}\varepsilon_n + \frac{E}{1-\nu^2}\varepsilon_s \\ \tau_{ns} &= \frac{E}{2(1+\nu)}\gamma_{ns} \end{aligned} \tag{7}$$

The term σ_s cannot be defined since the refined DEM only considers surface interaction. In addition, the Poisson effect cannot be considered since only direct interaction between two elements is considered, and indirect interaction is not considered. Therefore, the normal and shear stresses $\sigma_n(n)$ and $\tau_{ns}(n)$ are

$$\sigma_n = \frac{E}{1-\nu^2}\varepsilon_n \qquad \tau_{ns} = \frac{E}{2(1+\nu)}\gamma_{ns} \tag{8}$$

Substituting Eq. (8) into Eq. (3) and considering that the strains $\varepsilon_n(n)$ and $\gamma_{ns}(n)$ are derivatives of the displacements $u_n(n)$ and $u_s(n)$ concerning n, the forces are written as

$$\begin{aligned} f_n &= \frac{1}{\ell}\int_V \frac{E}{1-\nu^2}\varepsilon_n(a)dV = \frac{E}{(1-\nu^2)\ell}\int_V \frac{\partial u_n(a)}{\partial a}dV \\ f_s &= \frac{1}{\ell}\int_V \frac{E}{2(1+\nu)}\gamma_{ns}(a)dV = \frac{E}{2(1+\nu)\ell}\int_V \frac{\partial u_s(a)}{\partial a}dV \end{aligned} \tag{9}$$

The integrations in Eq. (9) can be conducted using the divergence theorem of Gauss. The volume integral is transformed into a surface integral. Assuming that the relative displacements $u_n(n)$ and

$u_s(n)$ are zero within the pyramid and only have the values u_n and u_s on the surface, only a surface integral at the surface is necessary. Eq. (9) can then be written as

$$f_n = \frac{E}{(1-\nu^2)\ell}\oint_S u_n(0)dS_n = \frac{E}{(1-\nu^2)\ell}u_n dA$$
$$f_s = \frac{E}{2(1+\nu)\ell}\oint_S u_s(0)dS_n = \frac{E}{2(1+\nu)\ell}u_s dA \quad (10)$$

where $\oint_S$ indicates surface integration, and dS_n is the area facing the n direction. Since the displacement at the surface is assumed to be constant, the surface integral is obtained as the product of displacement and the area. From this, the spring constants per area in the normal and shear directions, k_n and k_s, are found as follows.

$$k_n = \frac{E}{(1-\nu^2)\ell} \quad k_s = \frac{E}{2(1+\nu)\ell} \quad (11)$$

3.3 Springs Constant Between Elements

It is assumed that two elements, A and B, are continuous. Let ℓ_A be the distance from the gravity center of the element to the surface of element A in contact. Let ℓ_B be the distance from the gravity center to the surface of element B in contact. E_A and E_B are Young's moduli, and ν_A and ν_B are Poisson's ratios of elements A and B. The spring constants per area for the elements A and B are obtained from Eq. (11). Assuming that these springs are connected in series, the spring constants between elements per area, $\bar{k}_n$ and $\bar{k}_s$, are calculated as follows.

$$\bar{k}_n = \frac{1}{\frac{\ell_A}{E_A/(1-\nu_A^2)} + \frac{\ell_B}{E_B/(1-\nu_B^2)}}$$
$$\bar{k}_s = \frac{1}{\frac{\ell_A}{E_A/2(1+\nu_A)} + \frac{\ell_B}{E_B/2(1+\nu_B)}} \quad (12)$$

In this way, the interaction between the different materials is treated.

3.4 Damping Coefficient

When elements A and B, which are not connected by a restoring spring, come into contact or re-contact, a contact dashpot is installed between the elements parallel to the contact spring. The dashpot is introduced to express the energy dissipation of the contact.

Let the normal and tangential damping constants be h_n and h_s, and the damping coefficient per unit contact area be expressed as

$$c_n = 2h_n\sqrt{m_{ave}k_n} \quad c_s = 2h_s\sqrt{m_{ave}k_s}$$
$$m_{ave} = \rho_A\ell_A + \rho_B\ell_B \quad (13)$$

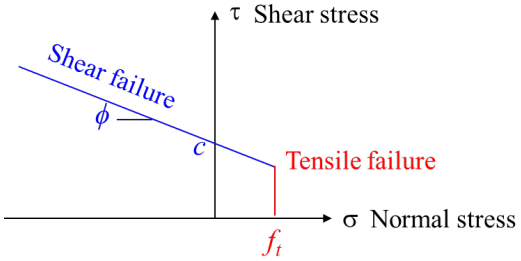

Fig.3 Modeling of failure phenomena

Here, m_{ave} is the equivalent mass per area relevant to this contact. ρ_A and ρ_B are the mass densities of elements A and B. A damping constant of 1.0 (critical damping) was adopted.

3.5 Modeling of Failure Phenomena

If the elongation of the restoring spring in the normal and shear directions is (u_n, u_s), the stress (σ, τ) in each direction can be expressed as

$$\sigma = \bar{k}_n u_n \quad \tau = \bar{k}_s u_s \quad (14)$$

where the stress in the normal direction is assumed to be positive in tension.

When the stress generated in the restoring spring reaches the elastic limit, the fracture phenomenon is represented by breaking the restoring spring. The elastic limit has criteria for tensile and shear failure.

Tensile failure occurs when the normal stress exceeds the tensile strength f_t. The yield function is given by (Fig. 3)

$$f_1(\sigma) = \sigma - f_t \quad (15)$$

As for shear failure, assuming that the bond strength is c and the friction angle is ϕ, the yield function is given by (Fig. 3)

$$f_2(\sigma) = |\tau| + \sigma\tan\phi - c \quad (16)$$

3.6 Upper Limit of Frictional Force

The restoring spring disappears once the failure occurs. A contact spring and a contact dashpot are generated during contact and re-contact. The contact spring is generated only when contact is made, so it is subject to compressive forces only. The contact force in the shear direction is assumed to be limited by the friction limit as follows, assuming the friction angle is ϕ.

$$\tau = \sigma\tan\phi \quad (17)$$

3.7 Equation of Motion

The force and moment acting on each element are the sums of the force and moment due to the restoring spring, contact spring, and contact dashpot, plus external forces such as gravity and seismic inertia force. The behavior of the distinct elements can be obtained by solving the equations of motion for the translational and rotational motion.

4. PROPOSED METHOD TO INTRODUCE POISSON EFFECT INTO REFINED DEM

4.1 Problems With the Refined DEM

As described, the refined DEM cannot consider the Poisson effect. When a compressive force is applied downward to two elements stacked in two layers, as shown in Fig.4(a), vertical strain due to compressive force can be expressed by overlapping the upper and lower elements, as shown in Fig.4(b). However, horizontal impregnation cannot be expressed because no force is generated between the elements in the horizontal direction. In the first equation of Eq. (8), normal strain ε_n due to normal stress σ_n is considered, but the orthogonal strain ε_s due to σ_n is ignored. It is clear from the formulation that the Poisson effect cannot be considered in the refined DEM.

4.2 Method for Introducing the Poisson Effect

The elasticity tensor $[D]$ is as follows.

$$[D]=\frac{E(1-\nu)}{(1+\nu)(1-2\nu)}\begin{bmatrix} 1 & \frac{\nu}{1-\nu} & \frac{\nu}{1-\nu} & 0 & 0 & 0 \\ \frac{\nu}{1-\nu} & 1 & \frac{\nu}{1-\nu} & 0 & 0 & 0 \\ \frac{\nu}{1-\nu} & \frac{\nu}{1-\nu} & 1 & 0 & 0 & 0 \\ 0 & 0 & 0 & \frac{1-2\nu}{2(1-\nu)} & 0 & 0 \\ 0 & 0 & 0 & 0 & \frac{1-2\nu}{2(1-\nu)} & 0 \\ 0 & 0 & 0 & 0 & 0 & \frac{1-2\nu}{2(1-\nu)} \end{bmatrix} \quad (18)$$

The non-diagonal component corresponding to the Poisson effect is extracted as $[D_P]$.

$$[D_P]=\frac{E(1-\nu)}{(1+\nu)(1-2\nu)}\begin{bmatrix} 0 & \nu/1-\nu & \nu/1-\nu & 0 & 0 & 0 \\ \nu/1-\nu & 0 & \nu/1-\nu & 0 & 0 & 0 \\ \nu/1-\nu & \nu/1-\nu & 0 & 0 & 0 & 0 \\ 0 & 0 & 0 & 0 & 0 & 0 \\ 0 & 0 & 0 & 0 & 0 & 0 \\ 0 & 0 & 0 & 0 & 0 & 0 \end{bmatrix} \quad (19)$$

Figure 5(a) shows eight distinct elements, two each in the width, depth, and height directions. The eight distinct elements are considered one set, and a hexahedron composed of vertices at each center of gravity of the discrete element is defined as a newly introduced finite element. In Figure 5(b), the elements in gray are the distinct elements, and the element in red is the finite element. The same procedure is applied to the entire analytical model to construct one finite element for each of the eight distinct elements.

As shown in Fig. 5(c), assume that the upper distinct elements move downwards by the vertical compressive force. Let the relative displacement vector of the eight vertices of the finite element (center of gravity of the eight distinct elements) be $\{\Delta u_P\}$, and the load vector due to the Poisson effect be $\{F_P\}$, then $\{F_P\}$ can be expressed by the following formula.

$$\{F_P\}=[K_P]\{\Delta u_P\} \quad (20)$$

$[K_P]$ is the contribution of the Poisson effect in the element stiffness matrix and obtained using the non-diagonal component of the elasticity tensor $[D_P]$.

$$[K_P]=[B]^T[D_P][B] \quad (21)$$

$[B]$ is a matrix that relates strain and displacement consisting of shape functions. From Eq. (20), the force acting on the center of gravity of each distinct element due to the Poisson effect can be calculated, and this is added to the equation of motion of each distinct element.

Figure 6 shows the numerical analysis flow of eight distinct elements, two each in the width (x), depth (y), and vertical (z) directions, that are compressed in the vertical direction. The elements shown by the gray lines in Fig. 6 are distinct elements, and the element shown by the red line is the finite element. The vertical movement of the distinct elements in the lowest row is assumed to be fixed. The numerical analysis flow is as follows.

Step 1: A downward force is applied to the upper distinct elements.

Step 2: The upper distinct elements move downward. The upper and lower distinct elements overlap, and the finite elements are accordingly compressed in the z direction.

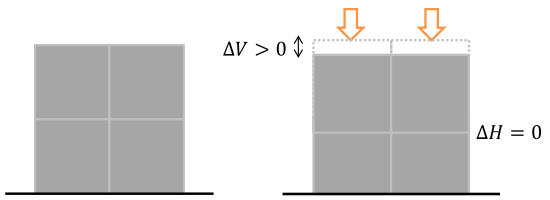

(a) Four-element model (b) Compressive force applied

Fig. 4 Reason why the Poisson effect cannot be expressed

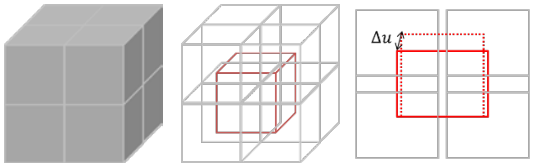

(a) Eight distinct elements (b)Finite element (c)Deformations of finite element

Fig. 5 How to consider the Poisson effect

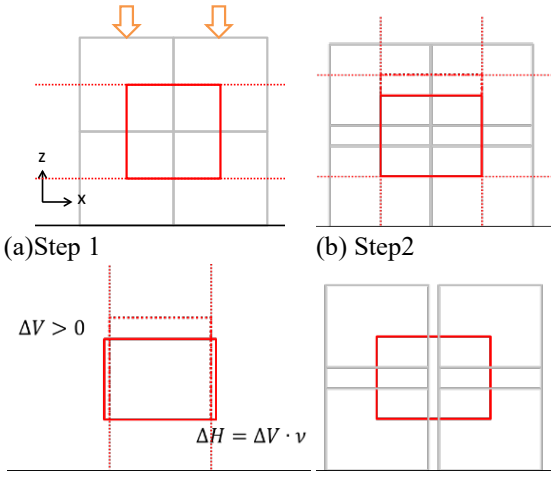

Fig. 6 Numerical analysis flow of expressing Poisson's effect due to compression behavior

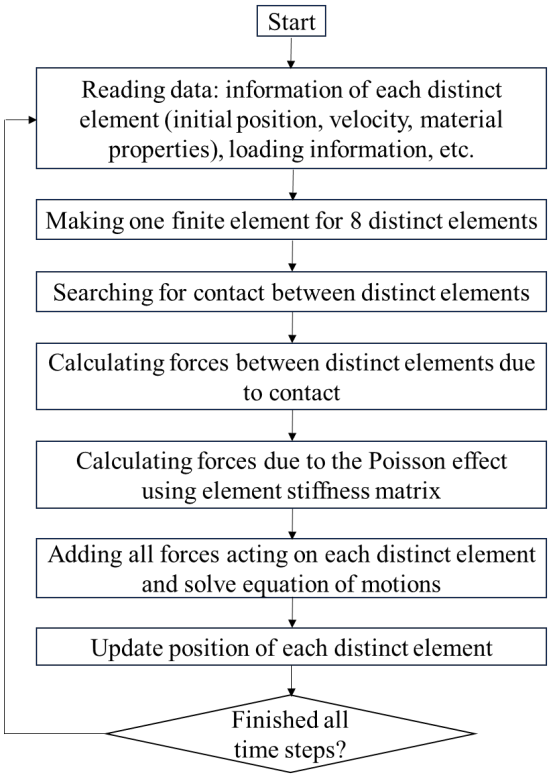

Fig.7 Numerical analysis flow

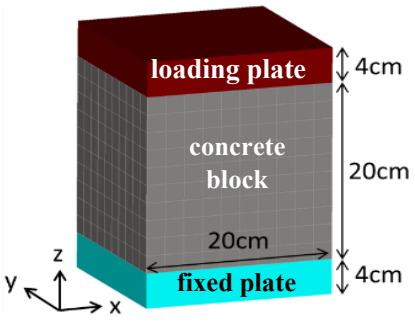

Fig. 8 Analysis model

Step 3: The force that causes the finite element to be impregnated in the x and y directions due to the Poisson effect is calculated by Eq. (20). This force is applied to the center of gravity of the distinct elements.

Step 4: The center of gravity of the distinct elements moves, and the behavior that the compressive force in the z direction reproduces the impregnation in the x and y directions can thus be traced.

The above process enables the proposed method to reproduce the impregnation caused by the Poisson effect. Figure 6 (d) shows the separation between the adjacent distinct elements in the x direction due to the Poisson effect. The Poisson effect creates a gap between the elements, which results in tensile stress between the elements. When the tensile stress is less than the tensile strength, it is considered that there is no tensile failure even though there is a gap between the elements. When the tensile stress exceeds the tensile strength of the element, a tensile failure is considered to have occurred, the restoring spring is broken, and cracks due to the Poisson effect are expressed.

4.2 Flow Chart of Numerical Analysis

Figure 7 indicates the numerical analysis flow of the proposed refined DEM considering the Poisson effect. The interaction force between distinct elements is estimated using finite elements.

5. NUMERICAL ANALYSIS OF COMPRESSION TEST OF A CONCRETE BLOCK

5.1 Overview

A numerical analysis of a compression test of a concrete block, shown in Fig. 8, is performed to verify whether the proposed method can reproduce tensile failure due to the Poisson effect. The concrete block is placed on a fixed element, and a loading plate is placed on top. The concrete block was subjected to compressive force by applying downward displacement to the loading plate. First, the horizontal-to-vertical relative displacement ratio was obtained and compared to the input Poisson's ratio value to confirm that the Poisson effect is reproduced. Then, it confirmed whether the tensile failure caused by the Poisson effect is reproduced.

5.2 Analysis Model

The concrete block shown in gray in Fig. 8 is a cube of 20 cm on each side, divided into 10 sections in the x, y, and z directions, and modeled with 1000

distinct elements. The loading plate shown in red and the fixed plate shown in light blue were modeled with the same width and depth as the concrete (20 cm) and height (4 cm) and were divided into 10 sections in the *x* and *y* directions and 1 section in the *z* direction. Each plate was modeled with 100 individual elements. The total number of elements is 1200 (10×10×12) distinct elements and 891(9×9×11) finite elements. The number of springs and dashpots on the element surfaces was 4 per side.

Table 1 shows the analytical parameters. Only tensile failure was considered, and shear failure was not allowed by setting the bond strength to infinity.

The loading plate was subjected to forced displacement at a rate of 1.0 mm/s in the negative *z* direction to apply a compressive force. The computation time interval was 2.0×10^{-6} s.

5.3 Analysis Results

5.3.1 Apparent Poisson's ratio

The apparent Poisson's ratio was calculated from the relative displacements of the centers of gravity of the three distinct elements indicated by the blue, yellow-green, and yellow circles in Fig. 9(a). The apparent Poisson's ratio was obtained by dividing the horizontal relative displacement between the blue and yellow elements by the vertical relative displacement between the blue and yellow elements. The results are shown in Fig.9(b). From 0 to 0.14 s, the apparent Poisson's ratio is almost the same as the input Poisson's ratio of 0.2. After 0.14 s, the apparent Poisson's ratio oscillates because tensile failure occurs, and a crack is formed between the blue and yellow-green elements.

5.3.2 Average compressive stress when a tensile fracture occurs

The reaction force from the concrete block on the loading plate when a tensile failure occurred (0.14 s) was divided by the cross-sectional area, and the compressive stress was found to be 2.12×10^7 N/m^2. The ratio of the tensile strength, 4.5×10^6 N/m^2, to the compressive stress, 2.12×10^7 N/m^2, is 0.21, which is similar to input Poisson's ratio of 0.2.

5.3.3 Failure situation

Figure 10 shows the tensile failure and horizontal impregnation when the downward displacement of 6.3 mm to 6.9 mm is applied. The width of the concrete block gradually increases, reproducing the impregnation of the concrete block in the horizontal direction. Clear vertical cracks are observed near the corner because the block is not restrained from the surrounding area. Figure 11 shows the results of compression tests conducted by the authors on a rectangular brick (10 cm wide, 6 cm deep, and 10 cm high), in which vertical cracks were observed, similar to the numerical results. The specimen differs in geometric dimensions from the block in the numerical example but is shown as an example of a compression test result for a rectangular block.

Table 1 Analysis parameters

(a)Material properties

Density	Young's modulus	Poisson's ratio
2.3×10^3 kg/m^3	3.0×10^{10} N/m^2	0.20

(b)Strength and damping coefficient of dashpot

Tensile Strength	Bond strength	Coefficient of friction	Damping coefficient
4.5×10^6 N/m^2	∞	0.624	1.0

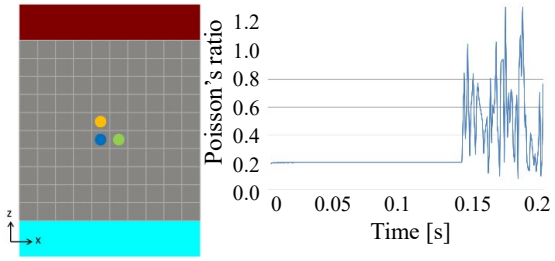

(a)Displacement extraction elements (b) Apparent Poisson's ratio

Fig. 9 Apparent Poisson's ratio

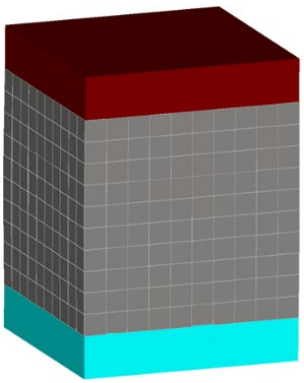

(a)At 6.3mm

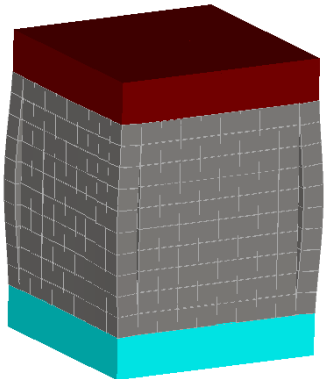

(b) At 6.9mm

Fig. 10 Tensile failure and horizontal impregnation due to the Poisson effect

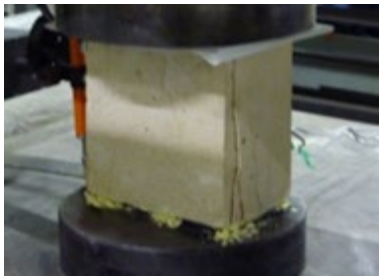

Fig. 11 Vertical cracks in bricks by a vertical compression test

6. CONCLUSIONS

The refined DEM, which models structures using rigid elements, has a problem in that it cannot consider the Poisson effect. In this study, the Poisson effect was introduced into the refined DEM to consider the tensile failure due to the Poisson effect. In the proposed method, the Poisson effect is expressed by setting up virtual finite elements in addition to the distinct elements. A new hexahedral finite element composed of the gravity centers of the eight distinct elements (2×2×2) is considered. Since the non-diagonal component of the elasticity tensor expresses the Poisson effect, the element stiffness matrix owing to the Poisson effect was developed using the non-diagonal component of the elasticity tensor. By multiplying the element stiffness matrix owing to the Poisson effect and the relative displacement vector, the force vector due to the Poisson effect was calculated and applied to the distinct elements.

The validity of the proposed method was verified by numerical analysis of a compression test on a cubic concrete block. The apparent Poisson's ratio was calculated as the horizontal-to-vertical relative displacement ratio, and it was found to be consistent with the input Poisson's ratio. Therefore, it was confirmed that the Poisson effect can be expressed. It was also confirmed that the compressive force causes tensile failure in the direction perpendicular to the compressive force. Thus, the tensile failure due to the Poisson effect can be expressed. In this way, the correct Poisson's ratio value was quantitatively reproduced, and tensile cracks due to compressive forces were qualitatively represented.

However, the current analysis code has the limitation that the element geometry of the refined DEM is limited to hexahedrons. The code needs to be improved so that it can be applied to arbitrary element shapes.

7. ACKNOWLEDGMENTS

This work is supported by JSPS KAKENHI Grand Number 23H01658.

8. REFERENCES

[1] OCHA (Office for the Coordination of Humanitarian Affairs): http://www.unocha.org/ (Last accessed: June 5, 2023).

[2] Furukawa A., Kiyono J., Parajuli R. R., Parajuli H. R., and Toki T., Evaluation of damage to an historic masonry building in Nepal through comparison of dynamic characteristics before and after the 2015 Gorkha Earthquake. Frontiers in the Built Environment, Vol.3, Issue 62, 2017, pp.1-16. https://doi.org/10.3389/fbuil.2017.00062

[3] Parajuli H. R., Kiyono J., Tatsumi T., Suzuki Y., Umemura H., Taniguchi H., Toki K., Furukawa A., and Maskey P. N., Dynamic characteristic investigation of a historical masonry building and surrounding ground in Kathmandu. Journal of Disaster Research, Vol. 6, No. 1, Dr6-1-4522, 2011, pp.1-10. http://dx.doi.org/10.20965/jdr.2011.p0026

[4] Parajuli R. R., Furukawa A., and Gautam D., Experimental characterization of monumental brick masonry in Nepal. Structures, Vol.28, 2020, pp.1314-1321. https://doi.org/10.1016/j.istruc.2020.09.065

[5] Kiyono J., and Furukawa A., Casualty occurrence mechanism in the collapse of timber-frame houses during an earthquake. Earthquake Engineering & Structural Dynamics, Vol.33, 2004, pp.1233-1248. http://dx.doi.org/10.1002/eqe.402

[6] Furukawa A., and Kiyono J., Casualty estimation in the collapse of masonry structures due to earthquake. Protection of Historical Buildings – Prohitech 09, Vol. 1 and 2, 2009, pp.423-429.

[7] Zienkiewicz O. C., and Taylor R. L., The Finite Element Method: Its Basis and Fundamentals. Butterworth-Heinemenn, Oxford, U.K., 2000, pp.1-756.

[8] Hori M., Oguni K., and Sakaguchi H., Proposal of FEM implemented with particle discretization for analysis of failure phenomena. Journal of the Mechanics and Physics of Solids, Vol.53, 2005, pp.681-703.

[9] Asai M., Yamashita K., Yamasaki Y., and Araki K., Estimation of Static and dynamic strength of stone arch bridges by using a discrete finite element model. Journal of Structural Engineering A, Vol.55A, 2009, pp.172-180.

[10] Shafee A., and Khoshghalb A., An improved node-based smoothed point interpolation method for coupled hydro-mechanical problems in geomechanics. Computers and Geotechnics, Vol.139, No.104415, 2021.

[11] Khoshghalb A., and Khalili N., An alternative approach for quasi - static large deformation analysis of saturated porous media using

meshfree method. International Journal for Numerical and Analytical Methods in Geomechanics, Vol. 39, Issue 9, 2015, pp.913-936.

[12] Dezfooli M.S., Khoshghalb A., Shafee A., and Khalili, N., An h-adaptive edge-based smoothed point interpolation method for elasto-plastic analysis of saturated porous media. Computers and Geotechnics, Vol.162, No.105628, 2023.

[13] Rabczuk T., and Belytschko T., A three-dimensional large deformation meshfree method for arbitrary evolving cracks. Computer Methods in Applied Mechanics and Engineering, Vol.196, No.29-30, 2007, pp.2777-2799.

[14] Cundall P. A., and Strack O. D. L., A discrete numerical model for granular assemblies. Geotechnique, Vol. 29, 1979, pp. 47-65.

[15] Furukawa A., Kiyono J., and Toki K., Proposal of a numerical simulation method for elastic, failure and collapse behaviors of structures and its application to seismic response analysis of masonry walls. Journal of Disaster Research, Vol.6, No.1, 2011, pp.51-68. http://dx.doi.org/10.20965/jdr.2011.p0051

[16] Lourenco P. B., Analysis of masonry structures with interface elements, theory and applications. Delft University of Technology, Faculty of Civil Engineering, TU-DELFT report no. 03-21-22-0-01, 1994, pp.1-34.

[17] Itasca, UDEC Universal Distinct Element Code: Theory and Background. Itasca Consulting Group Inc., Minneapolis, 2004.

[18] Furukawa A., Horikawa R., Kiyono J., and Toki, K., Seismic behavior analysis of masonry structures using the distinct element method considering element deformability. Journal of Natural Disaster Science, Vol.35, No.2, 2014, pp.43-53. https://doi.org/10.2328/jnds.35.43